ELSEVIER

Journal of Alloys and Compounds 243 (1996) 51–58

Journal of ALLOYS AND COMPOUNDS

Phase relations in the $MgMoO_4$–$Mg_3V_2O_8$ system and crystal structure of $Mg_{2.54}V_{1.08}Mo_{0.92}O_8$[1]

Xiandong Wang, Charlotte L. Stern, Kenneth R. Poeppelmeier*

Department of Chemistry, Northwestern University, Evanston, IL 60208-3113, USA

Received 15 April 1996; in final form 13 May 1996

Abstract

The phase relationships in the pseudobinary $MgMoO_4$–$Mg_3V_2O_8$ system have been determined by differential thermal analysis and X-ray diffraction analysis. The intermediate compound $Mg_{2.5}VMoO_8$ was found to exhibit a considerable solid solution $Mg_{2.5+x}V_{1.25}Mo_{1-2x}O_8$ ($-0.05 \leq x \leq 0.05$) at 1100 °C in air. Single crystals with composition of $Mg_{2.54}V_{1.08}Mo_{0.92}O_8$ were successfully grown from the Mg–V–Mo–Oxide flux. $Mg_{2.54}V_{1.08}Mo_{0.92}O_8$ crystallizes in the orthorhombic system, space group *Pnma* with $a = 5.058(1)$ Å, $b = 10.307(3)$ Å, $c = 17.402(4)$ Å, $Z = 6$. The vanadium and molybdenum cations remain in their highest oxidation states and charge neutrality associated with the variation of the V/Mo atomic ratio is balanced by an increase or decrease in the number of magnesium cations in the crystal.

Keywords: $Mg_{2.54}V_{1.08}Mo_{0.92}O_8$ and $MgMoO_4$–$Mg_3V_2O_8$ system; Phase diagram; Crystal structure

1. Introduction

Multicomponent vanadates or molybdates which contain isolated VO_4 or MoO_4 tetrahedra have attracted attention for their promising catalytic properties (high selectivity and conversion) for the dehydrogenation of alkanes [1–3]. One typical system is MgO–MoO_3–V_2O_5, in which $Mg_3V_2O_8$, $Mg_{2.5}VMoO_8$ and $MgMoO_4$ have shown good catalytic properties [3,4]. A study of the subsolidus-phase equilibria in the MgO–MoO_3–V_2O_5 system [5] revealed the coexistence of $Mg_3V_2O_8$ and $MgMoO_4$ with $Mg_{2.5}VMoO_8$. The structure of $Mg_{2.5}VMoO_8$ was modeled after $NaCo_{2.31}(MoO_4)_3$ [6] and solved by Rietveld refinement from X-ray powder diffraction data with an orthorhombic unit cell: $a = 5.0515(1)$ Å, $b = 10.3455(2)$ Å, $c = 17.4683(4)$ Å, $Z = 6$ in space group *Pnma*. In the present work, the phase diagram of the pseudobinary $MgMoO_4$–$Mg_3V_2O_8$ system was investigated by X-ray diffraction (XRD) and differential thermal analysis (DTA). The goal was to establish the relevant solid–liquid compatibilities in the $MgMoO_4$–$Mg_3V_2O_8$ system, to grow high quality single crystals in order to study thoroughly how partial occupancy of the magnesium sites maintains the vanadium and molybdenum cations in their highest oxidation state and preserves electrical neutrality.

2. Experimental

Pure $MgMoO_4$ and $Mg_3V_2O_8$ were prepared by solid state reaction from MgO (98%), V_2O_5 (99.6%) and MoO_3 (99.5%) (Aldrich Chemical Company, Inc.). DTA was conducted on a Thermal Analysis 2000 (Du Pont) instrument with alumina crucibles and Al_2O_3 powder as reference in a static air atmosphere. The measured temperatures were calibrated by melting gold (accuracy ±0.8 °C). For each composition, about 40 mg of thoroughly mixed powders of $MgMoO_4$ and $Mg_3V_2O_8$ were heated to 1200–1400 °C at a heating rate of 5 or 10 °C min^{-1}. To avoid the supercooling effect, the onset temperatures of endothermic peaks in DTA curves were chosen to determine the subsolidus and subliquidus temperatures, although the corresponding exothermic peaks were also detected when the samples were cooled from the highest temperatures. For compositions very close to the eutectic and peritectic points, owing to the overlap of the endothermic peaks in these cases, the separate

*Corresponding author.

[1]Dedicated to Professor Dr. Dr. h. c. Hans Georg von Schnering on the occasion of his 65th birthday.

0925-8388/96/$15.00
PII S0925-8388(96)02381-X

exothermic peaks were useful to estimate the liquidus temperatures. The samples used to determine the solubilities of solid solutions $Mg_{2.5+x}V_{1+2x}Mo_{1-2x}O_8$ were fired at 1100 °C for 55 h and quenched in air. For phase identification and lattice parameter calculations, X-ray powder diffraction data were collected on a Rigaku diffractometer (Cu Kα radiation, 40 kV, 20 mA, Ni filter, step scan 0.02°/10 s) in the 2θ range of 16–96°.

Based on the phase diagram of $MgMoO_4$–$Mg_3V_2O_8$ (see Fig. 1), a composition with 50 mol% $Mg_3V_2O_8$ was selected to grow $Mg_{2.5}VMoO_8$ single crystals. A ball-milled mixture (approximately 4 g) of $MgMoO_4$ and $Mg_3V_2O_8$ was packed into a platinum boat and covered with an alumina lid and heated at 120 °C h^{-1} to 1200 °C in air. After holding at 1200 °C for 12 min, the furnace was cooled to 1145 °C at 6 °C h^{-1} and subsequently to room temperature by turning power off to the furnace. Colorless or light yellow needle '$Mg_{2.5}VMoO_8$' crystals, ranging in size from about 0.2–0.5 mm wide and 2–5 mm long (see Fig. 2), were found distributed on the top of the melt. Under the optical microscope, many crystals appeared badly cracked, but several crystals were suitable for single-crystal diffraction. The total weight loss during the crystal growth was less than 0.2%, demonstrating that the vanadium and molybdenum species were not reduced during crystal growth.

A colorless and transparent '$Mg_{2.5}VMoO_8$' twin-free crystal with approximate dimensions of 0.03×0.08×0.4 mm^3 was selected for single-crystal diffraction and mounted on a glass fiber. All measurements were made on an Enraf–Nonius CAD4 diffractometer with graphite monochromated Mo Kα radiation. The data were collected at a temperature of −120±1 °C using the ω–θ scan technique to a maximum 2θ value of 49.9°. ω-scans of several intense reflections, made

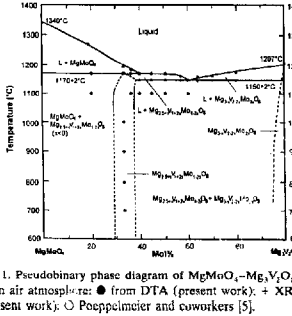

Fig. 1. Pseudobinary phase diagram of $MgMoO_4$–$Mg_3V_2O_8$ system in an air atmosphere: ● from DTA (present work); + XRD study (present work); ○ Poeppelmeier and coworkers [5].

Fig. 2. Optical photograph of the as-grown $Mg_{2.5+x}V_{1+2x}Mo_{1-2x}O_8$ crystals; scale in millimeters.

prior to data collection, had an average width at half-height of 0.30° with a take-off angle of 2.8°. Scans of (1.00+0.35 tanθ)° were made at a variable speed of 3.0–15.0° min^{-1} (in ω). Moving-crystal, moving counter background measurements were made by scanning an additional 25% above and below the scan range. Of the 1888 reflections collected, 1135 were unique (R_{int} = 0.023). The intensities of three representative reflections were measured after every 90 min of X-ray exposure time. No decay correction was applied. The linear absorption coefficient μ for Mo Kα radiation is 38.4 cm^{-1}. An analytical absorption correction was applied which resulted in transmission factors ranging from 0.77 to 0.92. The data were corrected for Lorentz and polarization effects. A correction for secondary extinction was applied.

The structure of '$Mg_{2.5}VMoO_8$' was solved by the direct method [7] and expanded using Fourier techniques [8]. The Mg and O atoms were refined with anisotropic thermal parameters while the disordered Mo and V atoms were refined with isotropic thermal parameters. The final full-matrix least squares refinement cycle based on 828 observed reflections ($I > 3.00\sigma(I)$) and 87 parameters converged (largest parameter shift was 0.00) with unweighted and weighted agreement factors of $R = \Sigma\|F_{obs} - F_{calc}\|/\Sigma F_{obs}$ = 0.027 and $R_w = [\Sigma w(F_{obs} - F_{calc})^2/\Sigma w F_{obs}^2]^{1/2}$ = 0.031 (with $w = 1/\sigma^2(F_{obs})$). The maximum and minimum peaks on the final difference Fourier map corresponded to 1.69 $e^- Å^{-3}$ and −1.01 $e^- Å^{-3}$ respectively. All calculations were performed using the TEXSAN crystallographic software package from Molecular Structure Corporation [9]. Crystal data and experimental details of the structure determination are compiled in Table 1.

The crystal faces were determined by axial photographs. The face perpendicular to the needle axis is

Table 1
Crystal data and details of $Mg_{2.54}V_{1.08}Mo_{0.92}O_8$ structure determination

Chemical formula	$Mg_{2.54}V_{1.08}Mo_{0.92}O_8$
Formular weight	333.01
Crystal system	orthorhombic
Space group	*Pnma* (No. 62)
a (Å)	5.058(1)
b (Å)	10.307(3)
c (Å)	17.402(4)
V (Å^3)	907.2(3)
Z	6
D_x, D_m [a] (g cm^{-3})	3.66, 3.68
μ (Mo Kα) (cm^{-1})	38.42
Approximate crystal dimensions (mm^3)	0.03×0.08×0.40
Radiation, wavelength (Å)	Mo Kα, 0.71069
Monochromator	graphite
Temperature (°C)	−120.0
Scan type	ω−θ
Scan width (deg)	(1.00 + 0.35tanθ)
$2\theta_{max}$ (deg)	49.9
Crystal to detector distance (mm)	21
Detector aperture (mm)	2.0–2.5 horizontal 2.0 vertical
No. of reflections measured	total: 1888 unique: 1135 (R_{int} = 0.023)
No. of observations ($I > 3.00\sigma(I)$)	828
No. of parameters	87
Residuals	
$R = \Sigma \lVert F_{obs} - F_{calc} \rVert / \Sigma F_{obs}$	0.027
$R_w = [\Sigma w(F_{obs} - F_{calc})^2 / \Sigma w F_{obs}^2]^{1/2}$	0.031
Goodness of fit factor	2.0

[a] See text.

the {100} plane; therefore, the fastest growing direction was [100]. The other two faces are {010} and {001}. The chemical composition of the investigated crystal was determined, after dissolving in nitric acid, by inductively coupled plasma atomic emission spectrophotometry (ICP-AES, Thermo Jarrell Ash, model Atomscan 25). The density was measured on single phase $Mg_{2.529}V_{1.059}Mo_{0.941}O_8$ at room temperature with apparatus described by Chern et al. [10].

3. Results and discussion

3.1. The $MgMoO_4$–$Mg_3V_2O_8$ phase diagram

The determined phase diagram of the pseudobinary $MgMoO_4$–$Mg_3V_2O_8$ system is represented in Fig. 1. One eutectic point was found at about 60 mol% $Mg_3V_2O_8$ and 1150±2 °C. The intermediate compound $Mg_{2.5}VMoO_8$ ($Mg_{2.5}V_{1+2x}Mo_{1-2x}O_8$ solid solution) melts incongruently at 1170±2 °C, which has been confirmed by DTA measurement on both the 33.33 mol% $Mg_3V_2O_8$ composition (corresponding to $Mg_{2.5}VMoO_8$) and the pre-reacted $Mg_{2.5}VMoO_8$. The subliquidus line within the crystalline zone of $Mg_{2.5}VMoO_8$ is rather flat and the temperature window is quite narrow ($\Delta T \leq 20$ °C). These results clearly indicate that: (1) the single crystals of $Mg_{2.5}VMoO_8$ cannot be grown by simple melting; (2) single crystals can be obtained within the composition range of about 37–60 mol% $Mg_3V_2O_8$ with slow cooling across the narrow temperature range 1170 to 1150 °C. The melting point of $Mg_3V_2O_8$ was determined to be 1207 °C, very close to the 1212 °C reported in the literature [11]. However, the observed melting point of $MgMoO_4$ was near 1340 °C which is 50 °C lower than that reported [12]. Finally, it should be noted that $Mg_{2.5}VMoO_8$ does not exhibit a phase transition up to 1100 °C when heated in air, thus $Mg_3V_2O_8$ (magnesium orthovanadate) and $Mg_{2.5}VMoO_8$ are both stable in one modification and melt incongruently.

3.2. Crystal structure refinement of $Mg_{2.54}V_{1.08}Mo_{0.92}O_8$

Prior to the determination of the exact composition of the studied crystal, the structure was modeled on the formula $Mg_{2.5}VMoO_8$. The vanadium and molybdenum atoms on the two tetrahedral sites (M1 and M2) are disordered (Fig. 3), i.e. they possess an equal occupancy on each site with a configuration of M1(0.25V+0.25Mo)+M2(0.5V+0.5Mo). Other possibilities, such as (i) M1(0.5V)+M2(0.25V+0.75Mo), (ii) M1(0.5Mo)+M2(0.25Mo+0.75V), (iii) M1(0.375V+0.125Mo)+M2(0.375V+0.625Mo) and (iv) M1(0.375Mo+0.125V)+M2(0.375Mo+0.625V) always gave higher R and R_w values as well as negative B_{iso} for M1 or M2 site. The configuration of

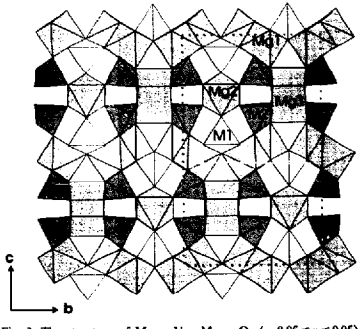

Fig. 3. The structure of $Mg_{2.5+x}V_{1+2x}Mo_{1-2x}O_8$ ($-0.05 \leq x \leq 0.05$) viewed approximately along the a axis showing two unit cells. Three types of MgO_6 polyhedron (Mg1, Mg2, Mg3) and two types of (V/Mo)O_4 tetrahedron (M1 = V1 + Mo1, M2 = V2 + Mo2) are marked.

M1(0.30V+0.20 Mo)+M2(0.45V+0.55Mo) can be rejected [13] at approximately the 0.01 level. The magnesium vacancies are predominately on the octahedral Mg2 sites when the minimization of R and R_w, goodness of fit indicator (GFI) and B_{eq} values (R = 3.2%, R_w = 3.9%, GFI = 2.49, B_{eq}(Mg2) = 1.50(6) and B_{eq}(Mg3) = 0.64(4)) are considered. Refinements with the magnesium vacancies on the trigonal prismatic Mg3 sites were not satisfactory (R = 4.0%, R_w = 5.2%, GFI = 3.31, B_{eq}(Mg2) = 2.9 and B_{eq}(Mg3) = −1.01). The latter model can be rejected [13] at the 0.005 level for the reduction in R (5.2/3.9 = 1.333), given 46 parameters and the total number of 828 observations. For similar reasons, magnesium vacancies could not be put on the Mg1 sites.

It was noted that by restraining B_{iso}(V) = B_{iso}(Mo) for both M1 and M2 sites, the refined structure had a formula $Mg_{2.62}V_{1.24}Mo_{0.76}O_8$ (R = 2.7%, R_w = 3.1%, GFI = 1.96). This indicated that the atomic ratio of V/Mo could be greater than 1:1. This assessment was subsequently confirmed by ICP analysis of the crystal used in the diffraction study. Chemical analysis revealed the atomic ratio was V:Mo = 1.00:0.86. Assuming V + Mo = 2, that is the M1 and M2 positions are fully occupied (this was confirmed by occupancy refinement), then the real composition of the crystal is $Mg_{2.54}V_{1.08}Mo_{0.92}O_8$. The structure was refined with this formula and with equal probability for vanadium or molybdenum atoms on both the M1 and M2 sites (i.e. M1(0.27V1+0.23Mo1) and M2(0.54V2+0.46Mo2)), and magnesium vacancies restricted to the Mg2 sites (refinement on magnesium occupancies gave 1.009, 0.420 and 0.499 for Mg1, Mg2 and Mg3 respectively, which reconfirms that the Mg vacancies are localized on the Mg2 site). The complete crystal data and details of $Mg_{2.54}Mo_{0.92}V_{1.08}O_8$ structure determination are summarized in Table 1. The measured density (3.68 g cm^{-3}) on $Mg_{2.529}V_{1.059}Mo_{0.941}O_8$ powder is in good agreement with the calculated density (3.66 g cm^{-3}) for $Mg_{2.54}V_{1.08}Mo_{0.92}O_8$ single crystal, considering the effects of small changes in composition and temperature. The atomic coordinates, anisotropic temperature factors and selected interatomic distances are given in Table 2, Table 3 and Table 4 respectively.

3.3. Description of the $Mg_{2.54}V_{1.08}Mo_{0.92}O_8$ structure

There are three crystallographically non-equivalent magnesium cations and two V/Mo positions (Table 2) in the asymmetric unit of the orthorhombic unit cell. The structure is formed from (V/Mo)O_4 tetrahedra, MgO_6 octahedra, and MgO_6 trigonal prisms (Fig. 3). The tetrahedra link zigzag sheets and columns formed by the octahedra and trigonal prisms respectively. The sheet is composed of zigzag chains formed by edge-sharing Mg1O_6 octahedra and each chain is joined to its neighbors on either side at intervals of a (Fig. 4). The isolated (V/Mo)O_4 tetrahedra, M1O_4 and M2O_4, are connected to the sheet of Mg1O_6 octahedra by sharing corners. M1O_4 seats in the triangular holes and M2O_4 lies on the top of the chain. M1O_4 tetrahedra are linked to the face-sharing Mg2O_6 octahedra from the top and bottom of the formed column (Fig. 5(a)) and M1, Mg2, and the shared oxygen are within same plane, parallel to the c axis (Fig. 3). M2O_4 tetrahedra are linked to the Mg2O_6 octahedra from sides (Fig. 5(b)). The edge-sharing Mg3O_6 trigonal prisms link to the isolated M2O_4 tetrahedra by sharing corners (Fig. 5(c)). Mg3O_6 trigonal prisms link to Mg1O_6 octahedra by sharing corners also. The overall structure can be viewed as isolated (V/Mo)O_4 tetrahedra joined to the inner wall of the hexagonal tunnels formed by the Mg1O_6 octahedra and Mg3O_6 trigonal

Table 2
Atomic coordinates, occupation factors and equivalent temperature parameters B_{eq} for the $Mg_{2.54}V_{1.08}Mo_{0.92}O_8$ structure

Atom	Wyckoff position	x	y	z	Occupation	B_{eq}/B_{iso} [a]
Mo(1)	4c	0.2184(1)	0.750	0.44364(4)	0.23	0.40(2)[b]
Mo(2)	8d	−0.2790(1)	0.47097(5)	0.34366(3)	0.46	0.48(2)[b]
V(1)	4c	0.2184(1)	0.750	0.44364(4)	0.27	0.40(2)[b]
V(2)	8d	−0.2790(1)	0.47097(5)	0.34366(3)	0.54	0.48(2)[b]
Mg(1)	8d	−0.2488(3)	0.5761(1)	0.52709(8)	1	0.85(3)
Mg(2)	4c	−0.0943(7)	0.750	0.2493(2)	0.405	2.27(6)
Mg(3)	4c	−0.7471(4)	0.250	0.3029(1)	0.50	0.96(4)
O(1)	8d	−0.0791(6)	0.3722(3)	0.2867(2)	1	1.05(6)
O(2)	8d	−0.3457(6)	0.6128(3)	0.2959(2)	1	1.13(6)
O(3)	8d	−0.0870(6)	0.5051(3)	0.4244(2)	1	0.83(6)
O(4)	8d	−0.5639(6)	0.3854(3)	0.3718(2)	1	0.89(6)
O(5)	4c	−0.0606(8)	0.750	0.5050(2)	0.50	0.81(9)
O(6)	8d	0.4129(6)	0.8848(3)	0.4643(2)	1	0.74(6)
O(7)	4c	0.1494(9)	0.750	0.3473(3)	0.50	1.10(9)

[a] $B_{eq} = \frac{8}{3}\pi^2[U_{11}(aa^*)^2 + U_{22}(bb^*) + U_{33}(cc^*)^2 + 2U_{12}aa^*bb^*\cos\gamma + 2U_{13}aa^*cc^*\cos\beta + 2U_{23}bb^*cc^*\cos\alpha]$.
[b] Isotropically refined atoms.

Table 3
Anisotropic displacement parameters for the $Mg_{2.54}V_{1.08}Mo_{0.92}O_8$ structure

Atom	U_{11}	U_{22}	U_{33}	U_{12}	U_{13}	U_{23}
Mg(1)	0.0063(7)	0.0110(8)	0.0149(8)	0.0001(6)	−0.0011(6)	−0.0028(6)
Mg(2)	0.053(2)	0.015(1)	0.018(1)	0.000	0.007(2)	0.000
Mg(3)	0.008(1)	0.014(1)	0.013(1)	0.000	−0.0011(9)	0.000
O(1)	0.010(2)	0.013(2)	0.017(1)	0.002(1)	−0.002(1)	−0.003(1)
O(2)	0.015(2)	0.016(2)	0.013(2)	0.000(2)	0.001(1)	−0.001(1)
O(3)	0.009(2)	0.011(1)	0.012(1)	0.002(1)	0.001(1)	0.000(1)
O(4)	0.011(2)	0.013(2)	0.011(2)	0.000(1)	−0.001(1)	0.000(1)
O(5)	0.006(2)	0.006(2)	0.020(2)	0.000	−0.001(2)	0.000
O(6)	0.008(2)	0.008(1)	0.012(1)	0.002(1)	−0.001(1)	−0.002(1)
O(7)	0.014(3)	0.011(2)	0.017(2)	0.000	−0.002(2)	0.000

Table 4
Selected interatomic distances (Å) and bond angles (deg) for $Mg_{2.54}V_{1.08}Mo_{0.92}O_8$

V(Mo)(1)	–O(5)	1.770(5)	O(5)–V(1)–O(6)	108.9(1) (2×)
	–O(6)	1.741(3) (2×)	O(5)–V(1)–O(7)	115.4(2)
	–O(7)	1.713(4)	O(6)–V(1)–O(7)	108.5(1) (2×)
V(Mo)(2)	–O(1)	1.744(3)	O(6)–V(1)–O(6)	106.1(2)
	–O(2)	1.716(3)	O(1)–V(2)–O(2)	109.9(2)
	–O(3)	1.745(3)	O(1)–V(2)–O(3)	104.6(1)
	–O(4)	1.758(3)	O(1)–V(2)–O(4)	109.8(1)
Mg(1)	–O(3)	2.095(4)	O(2)–V(2)–O(3)	109.0(2)
	–O(3)	2.072(4)	O(2)–V(2)–O(4)	113.7(2)
	–O(4)	2.038(3)	O(3)–V(2)–O(4)	109.4(1)
	–O(5)	2.066(3)		
	–O(6)	2.071(4)		
	–O(6)	2.142(4)		
Mg(2)	–O(2)	2.066(4) (2×)		
	–O(2)	2.049(4) (2×)		
	–O(7)	2.119(6)		
	–O(7)	2.106(6)		
Mg(3)	–O(1)	2.178(4) (2×)		
	–O(1)	2.117(4) (2×)		
	–O(4)	2.059(4) (2×)		
Mg(1)	–Mg(1)	3.131(3), 3.111(3)		
Mg(2)	–Mg(2)	2.5292(5)		
Mg(3)	–Mg(3)	3.128(3)		

prisms, with infinite columns of face-sharing $Mg2O_6$ octahedra passing through the center of the tunnels.

Orthorhombic $Mg_{2.54}V_{1.08}Mo_{0.92}O_8$ is very similar to $NaCo_{2.31}(MoO_4)_3$ [6] and $Cu_3Fe_4V_6O_{24}$ [14]. It is very interesting, in fact quite amazing, that the hexagonal motif can be preserved in compounds with such different chemical constituents. Their structural similarities and differences can be more readily understood by comparing the distinctive polyhedral units (Table 5) in these structures. The tetrahedral and trigonal prismatic (or related square planar sites in $Cu_3Fe_4V_6O_{24}$) positions are fully occupied. The cation deficiency occurs at the face-shared octahedral positions in $Mg_{2.54}V_{1.08}Mo_{0.92}O_8$ and $Cu_3Fe_4V_6O_{24}$. However, in $NaCo_{2.31}(MoO_4)_3$ it is likely to be distributed at both the face-shared and edge-corner-shared octahedral positions. The cation vacancies create undercoordinated basic oxygen atoms, which can be regarded as similar to those in the cation deficient spinel $Mg_3V_2O_8$ [15].

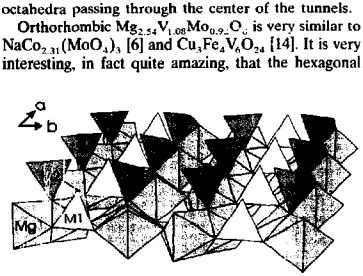

Fig. 4. The linkage between the $M1O_4$ and $M2O_6$ tetrahedra and $Mg1O_6$ octahedra.

Chains of face-sharing $Mg2O_6$ octahedra (see Fig. 5) are unusual and, to our knowledge, the chains are probably the first known example of magnesium octahedra arranged in this fashion. The distance between two adjacent Mg2 cations of 2.529 Å is con-

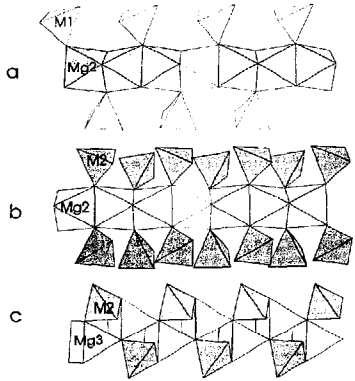

Fig. 5. The linkage of face-sharing $Mg2O_6$ octahedra with $M1O_4$ and $M2O_4$ tetrahedra by sharing corners are shown in (a) and (b) respectively. The linkage of edge-sharing $Mg3O_6$ trigonal prisms with $M2O_4$ tetrahedra by sharing corners is depicted in (c).

siderably shorter than Mg1–Mg1 (3.111–3.131 Å) and Mg3–Mg3 (3.128 Å), distances. In contrast, the metal–metal bonds in magnesium metal are 3.197 Å and 3.209 Å [16]. The *a* axis is twice the length of the Mg2–Mg2 bond. In $NaCo_{2.31}(MoO_4)_3$, the Co^{2+}–Co^{1+} cation–cation distance is 2.623 Å [6]; In $Cu_3Fe_4V_6O_{24}$, the Cu^{2+}–Cu^{2+} distance is 2.455 Å, which is even shorter than the Cu–Cu bond in the metal (2.556 Å [16]). It is noted that Mg2 on the 4*c* sites in $Mg_{2.54}V_{1.08}Mo_{0.92}O_8$ is present to about 4/5, higher than cobalt in $NaCo_{2.31}(MoO_4)_3$ (3/4) [6] and copper in $Cu_3Fe_4V_6O_{24}$ (3/5) [14]. The Mg2 cations exhibit large anisotropic displacement along the *a* axis and probably have some mobility along the *a* direction owing to the strong coulombic repulsion and cation vacancies. The, on average, short Mg2–Mg2 contact is the most likely explanation for the localization of the cation-deficiency on the Mg2 sites, rather than on the trigonal prismatic sites as suggested previously [5]. There are also four different Mg2–O distances (Table 4), rather than three as reported in Ref. [5].

Table 6
Comparison of the V/Mo–O bond lengths (Å) for the isolated $(V/Mo)O_4$ tetrahedra in the $Mg_{2.54}V_{1.08}Mo_{0.92}O_8$, $NaCo_{2.31}(MoO_4)_3$ and $Cu_3Fe_4V_6O_{24}$ structures

$NaCo_{2.31}(MoO_4)_3$		$Mg_{2.54}V_{1.08}Mo_{0.92}O_8$		$Cu_3Fe_4V_6O_{24}$	
$Mo1O_4$	$Mo2O_4$	$M1O_4$	$M2O_4$	$V1O_4$	$V2O_4$
1.817(16)	1.811(9)	1.771(5)	1.758(3)	1.763	1.776
1.761(13)	1.773(10)	1.740(3)	1.746(3)	1.730	1.745
1.760(10)	1.751(10)	1.740(3)	1.745(3)	1.730	1.704
1.760(10)	1.726(10)	1.711(4)	1.716(3)	1.688	1.671

Two M1–O (V/Mo–O) bonds have the same length (1.74 Å), which are on average shorter than the corresponding Mo–O bonds (1.76 Å) in $NaCo_{2.31}(MoO_4)_3$ and longer than the V–O bonds (1.73 Å) in $Cu_3Fe_4V_6O_{24}$ (Table 6). The degree of bond length variation for $M1O_4$ tetrahedra is approximately the same in the three cases. However, for $M2O_4$ tetrahedra, the two M2–O bond lengths that are very close to each other (1.745 Å, 1.746 Å) fall between the values observed for the MoO_4 and VO_4 examples. Interestingly, the total variation of the M2–O bond lengths (0.04 Å) is considerably smaller than that of Mo2–O (0.1 Å) and V2–O (0.1 Å) (Table 6). Thus, there is no reason to expect that the Mo^{6+} and V^{5+} cations will order in the isolated and well separated $(V/Mo)O_4$ tetrahedra.

The syntheses of $M_{2.5}VMoO_8$ (M = Zn and Mn) have been successful. $Mn_{2.5}VMoO_8$ is isostructural with $Mg_{2.5}VMoO_8$, but the symmetry of $Zn_{2.5}VMoO_8$ (space group $P2_12_12_1$) is reduced. Their crystal structures will be reported elsewhere [17].

3.4. The solid solution $Mg_{2.5+x}V_{1+2x}Mo_{1-2x}O_8$ $(-0.05 \le x \le 0.05)$

It is clear from the structural features of $Mg_{2.54}V_{1.08}Mo_{0.92}O_8$ that the change in charge owing to the increase of V/Mo atomic ratio is compensated by an increase in the magnesium content, that is reducing the concentration of magnesium vacancies on the Mg2 sites. If, for example, all the general and special positions are fully occupied (see Table 2), the ideal formula $Mg_{2.667}V_{1.333}Mo_{0.667}O_8$ (or $Mg_{16}V_8Mo_4O_{48}$) results. This means that, to a certain extent, a solid solution between $Mg_{2.5}VMoO_8$ and

Table 5
Comparison of cation–oxygen polyhedra for similar structures of $Mg_{2.54}V_{1.08}Mo_{0.92}O_8$, $NaCo_{2.31}(MoO_4)_3$ and $Cu_3Fe_4V_6O_{24}$

Octahedra 1	Octahedra 2	Trigonal prism or square planar	Tetrahrdra 1	Tetrahedra 2
$Mg1^{2+}O_6$	$Mg2^{2+}O_6$	$Mg3^{2+}O_6$ [a]	$M1^{5+/6+}O4$	$M2^{5+/6+}O_4$
$Co1^{2+}O_6$	$Co2^{2+/3+}O_6$	$Na^{+}O_6$ [a]	$Mo1^{6+}O_4$	$Mo2^{6+}O_4$
$Fe^{3+}O_6$	$Cu1^{2+}O_6$	$Cu2^{2+}O_4$ [b]	$V1^{5+}O_4$	$V2^{5+}O_4$

[a] Trigonal prism; [b] square planar.

$Mg_3V_2O_8$ or $MgMoO_4$ could form by varying the ratio of V/Mo (x can be positive or negative respectively). The existence of the $Mg_{2.5+x}V_{1+2x}Mo_{1-2x}O_8$ solid solution and the solubility limits have been determined by phase identification and lattice parameter calculations for a number of samples. One sample with the overall composition $Mg_{2.529}V_{1.059}Mo_{0.941}O_8$ (very close to the as-grown crystal $Mg_{2.54}V_{1.08}Mo_{0.92}O_8$), yielded a single phase without any $Mg_3V_2O_8$ present as a second phase, as judged by powder XRD. This result clearly indicates that a solid solution does exist, and is also consistent with the analyzed composition of the as-grown crystal. The remaining samples possess two phases, either $Mg_{2.5}VMoO_8$ and $Mg_3V_2O_8$ or $Mg_{2.5}VMoO_8$ and $MgMoO_4$. The calculated lattice parameters are presented in Fig. 6 for $-0.2 \leq x \leq 0.3$. A comparison of the single phase samples $Mg_{2.5+x}V_{1+2x}Mo_{1-2x}O_8$ ($x = 0.0$ and 0.029) indicates that the latter has an a axis about 0.005 Å longer, and b and c axes respectively about 0.01 Å and 0.02 Å shorter, than $Mg_{2.5}VMoO_8$. These trends, the expansion of the a axis and the contraction in the b and c axes, can be readily understood in terms of increased cation–cation repulsions and differing ion sizes $r(V^{5+}) < r(Mo^{6+})$ respectively. In contrast, when $x < 0$, the b and c lattice parameters increase and a remains nearly constant owing to increasing concentration of the larger cation Mo^{6+}. By extrapolation, the molybdenum-rich and vanadium-rich limits of the $Mg_{2.5+x}V_{1+2x}Mo_{1-2x}O_8$ solid solution were estimated to be $-0.05 \leq x \leq 0.05$. This result is in good agreement with the vanadium-rich composition of the as-grown crystals. Referring to Fig. 6, the b and c axes for $Mg_{2.54}V_{1.08}Mo_{0.92}O_8$ are about 10.33 Å and 17.44 Å respectively, which are larger than the single-crystal values (see Table 1) owing to the collection of data at different temperatures.

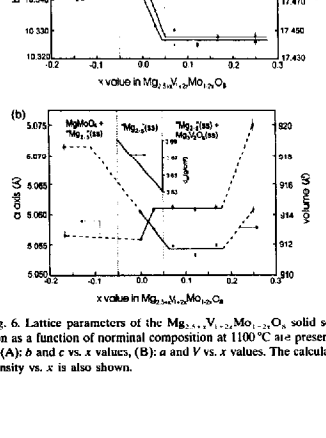

Fig. 6. Lattice parameters of the $Mg_{2.5+x}V_{1+2x}Mo_{1-2x}O_8$ solid solution as a function of nominal composition at 1100 °C are presented in (A): b and c vs. x values, (B): a and V vs. x values. The calculated density vs. x is also shown.

4. Conclusions

The phase diagram of the pseudobinary $MgMoO_4$–$Mg_3V_2O_8$ system has been established by DTA and XRD analyses. A solid solution $Mg_{2.5+x}V_{1+2x}Mo_{1-2x}O_8$ ($-0.05 \leq x \leq 0.05$) was found wherein the variation of atomic ratio V/Mo is exactly compensated by the magnesium cation concentration. The crystal structure of $Mg_{2.5+x}V_{1+2x}Mo_{1-2x}O_8$ ($x = 0.04$) was solved by single-crystal XRD and compared with the mixed valent $Co^{2+/3+}$ and cobalt deficient $NaCo_{2.31}(MoO_4)_3$ and the Cu^{2+} copper deficient $Cu_3Fe_4V_6O_{24}$.

Acknowledgments

The authors wish to thank Kevin R. Heier and Dr. Larry Cirjak for discussions and acknowledge an Extramural Research Award (EMRA) from BP America, Inc., the National Science Foundation (NSF) (No. DMR-9412971) and the MRC of Northwestern University supported by NSF (No. DMR-9120521) for support of this research work.

References

[1] G.A. Stepanov, A.L. Tsailinggol'd, V.A. Levin and F.S. Pilipenko, *Stud. Surf. Sci. Catal. B, 7* (1981) 1293.
[2] M.A. Chaar, D. Patel, M.C. Kung and H.H. Kung, *J. Catal., 105* (1987) 483.
[3] W.D. Harding, H.H. Kung, V.L. Kozhevnikov and K.R. Poeppelmeier, *J. Catal., 144* (1993) 597.
[4] S.C. Chang, M.A. Lenger and M.R. Bare, *J. Phys. Chem., 96* (1992) 10358.
[5] V.G. Zubkov, I.A. Leonidov, K.R. Poeppelmeier and V.L. Kozhevnikov, *J. Solid State Chem., 111* (1994) 197.
[6] J.A. Ibers and G.W. Smith, *Acta Crystallogr., 17* (1964) 190.
[7] G.M. Sheldrick, SHELX86, in G.M. Sheldrick, C. Kruger and R. Goddard (eds.), *Crystallographic Computing 3*, Oxford University Press, 1985, p. 175.
[8] P.T. Beurskens, G. Admiraal, G. Beurskens, W.P. Bosman, S. Garcia-Granda, R.O. Gould, J.M.M. Smits and C. Smykalla, DIRDIF92, in *The DIRDIF program system*, Technical Report of the Crystallography Laboratory, University of Nijmegen, Netherlands, 1992.

[9] TEXSAN-TEXRAY Structure Analysis Package, Molecular Structure Corporation, 1985.
[10] M.Y. Chern, R.D. Mariani, D.A. Vennos and F.J. DiSalvo, *Rev. Sci. Instrum.*, *61* (1990) 1733.
[11] A.A. Fotiev, B.V. Slobodin and M.Ya. Khodos, in *Vanadates: Composition, Structure, Properties*, Science, Moscow, 1988.
[12] V.M. Zhukovski, *Dissertation*, Ural State University, Sverdlovsk, 1974.
[13] W.C. Hamilton, *Acta Crystallogr.*, *18* (1965) 505.
[14] J.M. Hughes, S.J. Starkey, M.L. Malinconico and L.L. Maliconico, *Am. Mineral.*, *72* (1987) 1000.
[15] N. Krishnamachari and C. Calvo, *Can. J. Chem.*, *49* (1971) 1629.
[16] W.B. Pearson (ed.), in *Handbook of Lattice Spacings and Structures of Metals*, Vol. 2, Pergamon, 1967, p. 80.
[17] X.D. Wang, K. Heier, C.L. Stern and K.R. Poeppelmeier, in preparation.